CHEMISTRY OF MATERIALS

Article

pubs.acs.org/cm

Synthesis and Low Temperature In Situ Sintering of Uranium Oxide Nanoparticles

Tina M. Nenoff,*[,†] Benjamin W. Jacobs,[‡] David B. Robinson,[‡] Paula P. Provencio,[§] Jianyu Huang,[§] Summer Ferreira,[†] and Donald J. Hanson[⊥]

[†]Department of Surface and Interface Sciences, MS-1415, [§]Center for Integrated Nanotechnologies, MS-1314, and [⊥]Department of Hot Cells and Gamma Facilities, MS-1143, Sandia National Laboratories, P.O. Box 5800, Albuquerque, New Mexico 87185, United States

[‡]Department of Energy Nanomaterials, MS-9291, Sandia National Laboratories, P.O. Box 969, Livermore, California 94551-0969, United States

Supporting Information

ABSTRACT: The recycling and reuse of uranyl salt solutions produced from the acid dissolution of spent nuclear fuels is of particular interest for the reprocessing of nuclear fuels. The ability to utilize these dissolved salts as precursors for bulk UO_2 defines a materials pathway for the reduction of nuclear waste destined for long-term repository storage. We present a room temperature (RT) synthesis of uranium dioxide nanoparticles (NPs) in acidic solutions, whose small size and uniform shape allow for dramatic decreases in sintering temperature. Gamma irradiation is a valuable method for the synthesis of a wide range of metal-based NPs. Here it has been successfully used to form (depleted) uranium oxide (d-UO_2) NPs. In particular, this study focuses on the reaction dependency of solution pH and reaction dose on the shapes, sizes, yield, and properties of the products. The thermal stability and sintering behavior of the d-UO_2 NPs is studied utilizing transmission electron microscopy (TEM) with an in situ heating stage. These d-UO_2 NPs exhibit sintering temperatures in the range of 500 °C–600 °C, which is between 700–1000 °C lower than reported bulk UO_2 sintering temperatures. Detailed characterization results from UV–vis spectroscopy, TEM, and in situ heating stage TEM are presented for the reaction solutions, the RT NP products, and the sintered NPs.

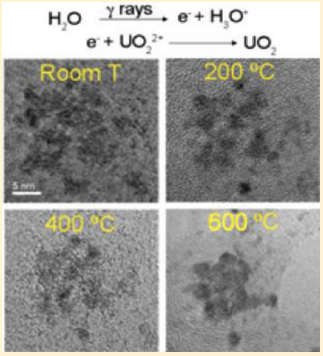

KEYWORDS: *radiolysis, uranium oxide, UO_2, sintering, nanoparticle*

INTRODUCTION

Metal and metal oxide nanoparticles (NPs) have high and often tunable surface energies per unit volume, a property that allows them to be flexibly manipulated and consolidated under mild thermal and chemical conditions. This is of potential value in the high temperature processing of actinide mixtures to mixed oxide fuels. It can be very difficult to produce phase-pure mixed oxide bulk phases as the components have great variation in their thermal properties; traditional high temperature sintering may result in volatilization of component oxides, rendering the bulk product mixed oxide inconsistent in composition. Many standard approaches to NP synthesis, such as room temperature (RT) chemical reduction by borohydride in the presence of surfactants, are ineffective when applied to acidic actinide solutions with very low reduction potentials, and can introduce byproducts that are difficult to remove.

Radiolysis is a RT procedure for the synthesis of NPs. Recently, it has been used in the synthesis and study of metallic,[1] and particularly alloyed,[1−5] NPs. This method provides a strong reducing environment that allows for the formation of NP products that are uniform in size, shape, and composition. While there has been significant investigation of aqueous uranium chemistry, including the formation of uranyl nanoclusters,[6] and the effect of alpha[7] and gamma (γ) irradiation on U oxidation states,[8,9] there has been very little reported on NP synthesis from actinide precursors via γ-irradiation.[10] We expect that the use of radiolysis for actinide NP formation will allow for precise control of product composition. Furthermore, the uniform size and shape of NPs formed should allow for a lowering in temperature for NP consolidation and sintering. This is of particular interest for the recycling and reuse of uranyl salt solutions produced from the acid dissolution of spent nuclear fuels; the dissolved salts can be used in the formation of UO_2 NPs and then sintered into bulk uranium oxide for reuse in mixed oxide fuels.

In the formation of NPs under radiolysis, γ-irradiation creates hydrated electrons, H atoms, and hydroxyl radicals in the aqueous reaction solution (see eq 1):

$$H_2O \Rightarrow e^-_{aq},\ H_2,\ OH^\bullet,\ H^\bullet,\ H_3O^+ \quad (1)$$

Hydrated electrons reduce metal (M) ions in solution to produce metal NPs (see eq 2):

Received: July 19, 2011
Revised: October 14, 2011
Published: November 15, 2011

$$M^{n+} + ne^-_{aq} \Rightarrow M^0 \quad (2)$$

The reported NPs formed via radiolysis[1−4] are composed of metals whose standard redox potentials are no more than a few hundred millivolts more negative than water and show stability when alloyed in NPs with more noble metals. Contrary to this, actinides have standard reduction potentials about 2 V more negative than water,[11] presenting a challenge to the formation of stable metallic particles in water. However, under certain conditions, some intermediate oxidation states of actinides are rendered insoluble or are able to form colloids in an aqueous environment. The use of γ-irradiation as a method to form a highly reducing aqueous environment can be a convenient pathway to the formation of the actinide colloids. Research by Roth et al.[10] has shown that the use of radiolysis has led to the successful reduction of uranyl (UO_2^{2+}) ions to UO_2 NPs, although limitations on yield were encountered. The specific reaction (see eq 3) expected in this case is:

$$UO_2^{2+} + 2e^-_{aq} \Rightarrow UO_2(s) \quad (3)$$

We are pursuing a combination of low temperature synthesis of the uranium dioxide NPs with low temperature NP sintering as a preferred pathway to reuse of the oxide for fuels; by dramatically lowering the sintering temperature to below 700 °C, volatilization of certain actinide oxide components can be avoided. Sintering of NPs may be achieved at lower temperatures than for micrometer or larger sized particles.[12,13] Low temperature sintering usually requires hot pressing techniques, the addition of a dopant to prevent extensive grain growth, or seeds to control transformations.[14] However, successful approaches to low temperature sintering have been achieved for certain NP oxides (e.g., zirconia) through either cold isostatic pressing followed by sintering[14] or with spark plasma sintering.[15]

With respect to UO_2, micrometer-sized particles have traditionally been shown to sinter at 1500 to 1700 °C.[16] Lower sintering temperatures have been demonstrated for smaller UO_2 particles, with higher specific surface area (SSA); sintering at as low as 1300 °C was observed with UO_2 particles having a SSA of 20 m^2/g (which corresponds to about 30 nm particles assuming spherical particles with 11 g/cm^3 density).[17] It is anticipated that UO_2 NPs with even smaller SSA (5−10 nm in diameter, and about 100 m^2/g as spheres) can be sintered at dramatically lower temperatures. Furthermore, recent reporting shows that through the simple use of an in situ heating stage in transmission electron microscopy (TEM), sintering of both nanoporous Pd NPs and Pd-alloy NPs can be observed in real time.[18]

Herein, we describe the use of radiolysis for the RT synthesis of uranium oxide NPs in acidic aqueous solutions, adjusting pH and spectroscopically tracking reactant and product species. Characterization of the NPs is achieved with the use of UV−vis and high resolution TEM (HRTEM). Consolidation and sintering of the NPs at dramatically reduced temperatures from those of micrometer sized UO_2 is demonstrated in the TEM using an in situ heating stage.

EXPERIMENTAL SECTION

Sample Preparation. Only depleted uranium containing reactants were used for all experiments. Twenty milliter samples were prepared that consist of 10 mM uranyl nitrate, $UO_2(NO_3)_2{\cdot}6H_2O$ (International Bio-Analytical Industries) in aqueous solutions of deionized water with 10% isopropanol. Reagents are from Aldrich unless otherwise specified. No surfactants were used during the NP synthesis, as done in previous radiolysis experiments,[3,4] because surfactants may hinder the NP sintering step and can be challenging to remove. The samples were prepared in specially made glassware: 100 mL vessels with quartz cuvette side arms having a 0.5 cm optical path length. The solutions were prepared in these vessels. All as-prepared samples were pH = 3.0. Samples were adjusted lower to pH = 1.2 using 0.1 M HNO_3, and to pH = 1.5 using 0.1 M HCl. Samples adjusted higher to pH 4.0 were prepared using 0.1 M KOH. The two outlets to the vessel were sealed with rubber stoppers and wrapped in parafilm. The solutions were deaerated by bubbling argon for 15 min through the solution prior to irradiation. Samples were irradiated at the Sandia National Laboratories' Gamma Irradiation Facility (GIF) using a ^{60}Co-γ source. All samples were exposed to 5.5 rad/s (198 Gray/h) for at least 7 days; some samples were irradiated for an additional 3 days (10 days total). Dose rate was calculated based on distance from the source and confirmed by dosimetry.

Characterization. Ultraviolet−visible (UV−vis) spectroscopy and TEM techniques were used to analyze the solutions, NPs, in situ sintering behavior, and sintering products. Both before and after irradiation, the samples were analyzed with UV−vis spectroscopy using a Varian Cary 300 Scan UV−visible Spectrophotometer. pH was measured using an Accumet Model 20 pH meter. Because of the reaction vessel design, UV−vis spectroscopy was carried out without the need to open the vessel and expose the reaction to oxygen. Using a straight line fit between 396 and 435 nm, the area under the curves was calculated for the uranyl ion peaks for samples at pH = 1.2, 1.5, and 3.0. This method is expected to underestimate the ion concentration in solution. However, because of the red shift in the UV absorption onset upon NP formation from about 350 to 390 nm, it is not possible to deconvolve the NP absorption from ion absorption making precise calculations of the reaction completion impossible.

General TEM characterization was carried out on carbon TEM grids with a Tecnai G(2) F30 S-Twin 300 kV TEM (FEI Company). TEM sample grids were made in glovebags under flowing nitrogen; reaction solutions were never exposed to air post-irradiation. Approximately 10 μL of product solution was dripped onto the grid and allowed to dry prior to data collection.

In situ sintering and simultaneous NP characterization were done on a JEOL 2010F field emission microscope operating at 200 kV in bright field mode (BF), using Protochips TEM HF1R1 grids. These grids have an intercalated electrode design across the imaging area of the grid to provide uniform and rapid heating, and are mounted on a Protochips Aduro holder. Temperatures were stepped from RT to the predetermined temperature, held for 30 s, and stepped back to RT, successively, to 200 °C, 300 °C, 400 °C, *400 °C, 500 °C, *500 °C, and *600 °C, where heat treatments denoted by an * symbol were carried out for 60 s. High resolution TEM analysis was carried out between heat treatments. Energy Dispersive Spectrometry (EDS) is carried out using an Oxford Inca X-Sight system. Diffraction measurements were taken before and after heat treatment at 150 cm^{-1} and 200 cm^{-1} camera lengths with conversion factors of 0.0183 nm^{-1}/pixel and 0.0232 nm^{-1}/pixel respectively.

RESULTS

Our studies show that reaction pH plays a key role in the NP formation of uranium dioxide by radiolysis. Through the use of UV−vis spectroscopy, the extent of reaction completion and product yield can be determined. The NP presence and particle size, and the influence of particle size and shape on sintering properties, are studied by TEM.

NPs. The UV−vis spectroscopy of each uranyl nitrate solution is taken before irradiation and at 7 days after irradiation; in an effort to study effects of additional radiation on particle growth, UV−vis spectra from some samples were also taken after an additional 3 days of irradiation (total 10 days). In preirradiation solutions of samples prepared at pH =

1.2, 1.5, and 3.0, there is a set of three peaks with the largest, central peak at 413.8 nm (Figure 1). The peak at 413.8 nm is

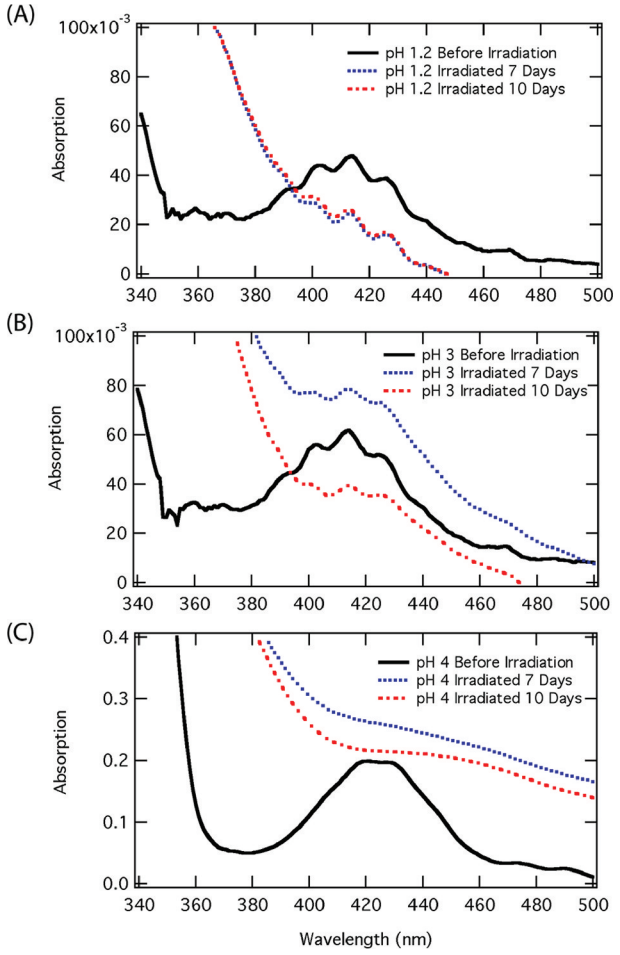

Figure 1. UV−vis spectroscopy of uranyl nitrate solutions (A) at pH = 1.2 adjusted with HNO_3, (B) pH = 3.0, and (C) pH = 4.0 adjusted with KOH. Black curves denote solutions before irradiation. Blue dotted lines plot spectra after 7 days of irradiation at 5 rad/s, red dashed lines denote spectra after 10 days of irradiation at 5 rad/s.

characteristic of UO_2^{2+}.[19] These peaks indicate precursor uranyl nitrate salts in solution. After 7 days of irradiation, the absorption edge in the UV is red-shifted, consistent with NP formation. The uranyl ion peaks are still present, but with lower intensity because of the conversion of a fraction of the uranyl ions to uranium oxide.

For the sample at pH = 1.2, three additional days of irradiation on the sample (10 days of total irradiation) resulted in no further reduction of the 413.8 nm peak from the 7 day irradiation results (see Figure 1A). This indicates two key points: the reaction will not convert further at this dose rate, and some reactant ions remain unreacted in solution. The approximated conversion of uranyl ions to UO_2 NPs is calculated to be 70% after 7 days, and with additional no change after 10 days of irradiation.

These results are consistent with the Pourbaix diagram for aqueous uranium oxide complexes in the absence of strong coordinating groups at pH = 1.2. Under irradiation, the solution is not equilibrated at a defined redox potential, but low potentials within the window of water stability can be considered relevant here.[20] The Pourbaix diagram predicts the presence of insoluble UO_2, but also partial hydrolysis of uranium−oxygen bonds in this range to form soluble U(IV) species, and suggests that the uranyl ion is favored at higher potentials, so these species can be expected to coexist after long reaction times. By contrast, samples adjusted with hydrochloric acid to pH 1.5 show much lower conversion or uranyl nitrate (Figure 2), with only 17% converting to UO_2 after 7 days of

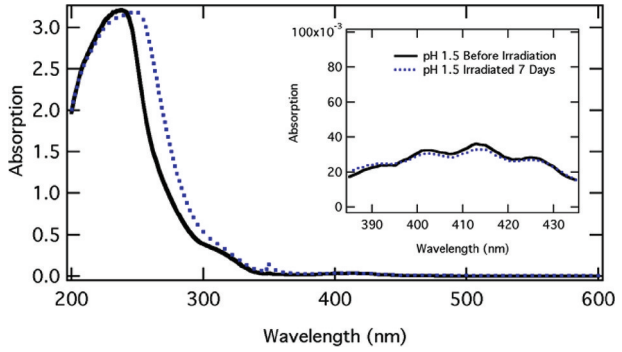

Figure 2. UV−vis spectroscopy of uranyl nitrate solutions (A) at pH = 1.5 adjusted with HCl. Black curve denotes solution before irradiation. Blue dotted line plots spectra after 7 days of irradiation at 5 rad/s. Inset plots of the irradiated spectra scaled to a straight-line fit with the unirradiated spectra between 396 and 435 nm wavelengths.

irradiation. It is known that chloride affects the uranium chemistry, and the equilibrium products may be strongly affected by the presence of chloride.[9]

In the pH = 3.0 preirradiated sample, there is a similar UV−vis peak at 413.8 nm (Figure 1B). The UV−vis exhibits a large absorption edge in the UV that red shifts from 350 to 390 nm, again indicative of UO_2 NP formation. There is significant background absorption across all wavelengths; the solution appears partially opaque, which we attribute to small aggregates that did not settle out of solution prior to measurement. After 10 day irradiation, the sample was left to sit overnight, allowing aggregates to settle out before the solution spectra was taken, leading to a significant reduction in the background absorption. A small peak at 413.8 nm is still observed in the UV−vis spectrum, suggesting that the uranyl ions have not been fully reduced to uranium oxide, as was observed in the lower pH samples. The area under the curves was calculated for the uranyl ion peaks, which corresponded to a 49% and 79% reduction after 7 and 10 days of irradiation, respectively. The increased scattering present in the 7 day sample likely caused errors in the calculated ion concentration for that time period.

In the sample at pH = 4.0, the reaction solution is slightly opaque upon initial preparation (see Supporting Information, Figure S1), and a scattering background is observed in the UV−vis spectrum. Otherwise, the UV−vis data show peaks at 421 and 429 nm, both of which are an order of magnitude higher than seen for lower pH samples (Figure 1C). These peaks indicate hydroxylated uranyl ions of $(UO_2)_2(OH)_2^{2+}$ and $(UO_2)_3(OH)^{5+}$, respectively, which have greater absorbance than UO_2^{2+}.[19] After both 7 and 10 days of irradiation, the solutions are opaque, with no precipitate settlement even after several days. UV−vis peaks indicative of the hydroxylated ions are not visible after irradiation, providing evidence of near complete reduction of the ions to UO_2. As in lower pH samples, a red shift in the absorption edge at short wavelengths (from 360 to 400 nm in this case) indicates NP formation.

dx.doi.org/10.1021/cm2020669 | Chem. Mater. 2011, 23, 5185−5190

Attempts were made to study higher pH solutions. However, all of these reaction solutions resulted in large precipitates prior to irradiation; no homogeneous reaction media were obtained, and no pure NP solutions were formed with irradiation. Stable colloids or suspensions are expected at low ionic strength when particles have a net charge. The isoelectric point (IEP) of UO_2 is at pH = 5.0−5.5,[21] so at pH greater than 4.0, the particles are expected to have no net charge, or if negatively charged, to be aggregated by the divalent uranyl cations.

NPs and Sintering. With in situ heating stage TEM, the change in size and shape of NPs through sintering can be observed. d-UO_2 NP samples from solutions at pH = 1.5, 3.0, and 4.0 were studied for sintering.

The irradiation of solutions at pH = 1.5 form small NPs that average 3 nm in diameter (Figure 3A). After in situ heating the sample to 600 °C, the NPs and their lattice fringes become clearer, indicating that the NPs have grown in size to approximately 5 nm in diameter (Figure 3B). Initially, there are two weak diffuse rings observed in the diffraction pattern of the as-made NPs (Figure 4A), indicative of small grains and possibly some amorphous particles. After sintering, the diffraction pattern is considerably more distinct, with an increase in the number of rings, each of which is sharper and stronger (Figure 4B). Because the NPs are on the TEM grid during heating and subsequent sintering, the extent of NP growth is limited by the availability of neighboring particles. However, we expect the kinetics and mechanism of growth to be similar to those of a bulk sample.

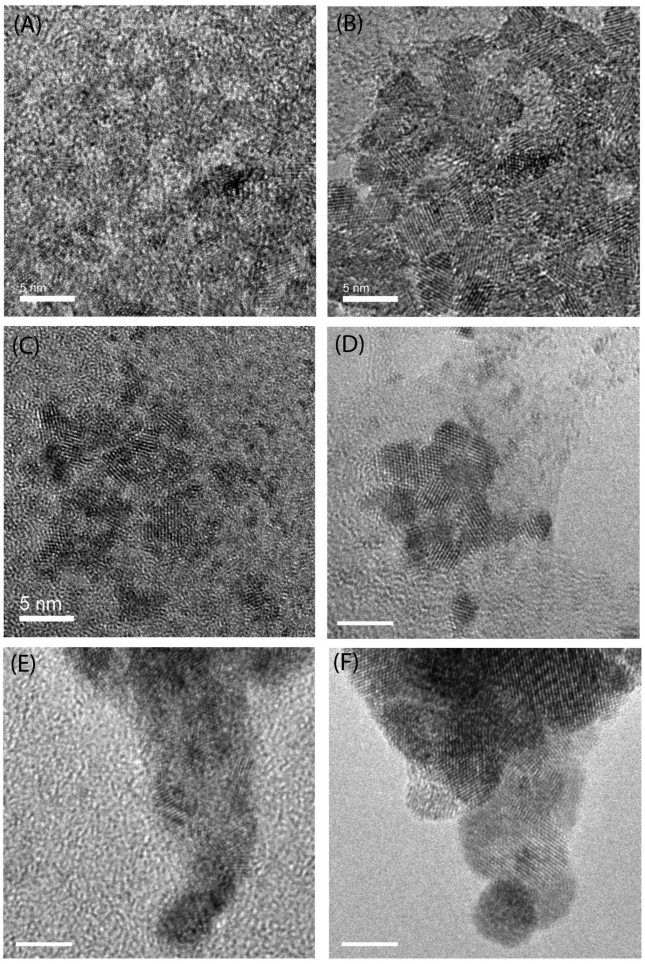

Figure 3. TEM images of UO_2 NPs formed at pH = 1.5 with 7 days of irradiation (A) before heating and (B) after heating to 600 °C; at pH = 3.0 with 7 days of irradiation (C) before heating and (D) after heating to 500 °C; at pH = 4.0 with 10 days of irradiation (E) before heating and (F) after heating to 600 °C.

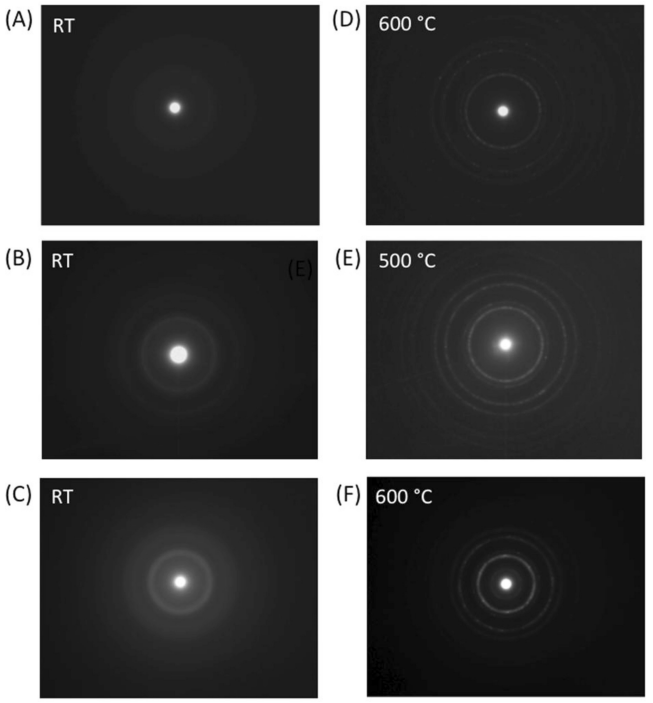

Figure 4. TEM diffraction patterns of UO_2 NPs formed at pH = 1.5 with 7 days of irradiation (A) before heating and (B) after heating to 600 °C; at pH = 3.0 with 7 days of irradiation (C) before heating and (D) after heating to 500 °C; at pH = 4.0 with 10 days of irradiation (E) before heating and (F) after heating to 600 °C.

The irradiation of solutions at pH = 3.0 form NPs that are slightly larger in diameter (≈3.5 nm) than the samples at pH = 1.5 (Figure 3C). With heating to 500 °C, analysis of the TEM data indicates the individual NPs have grown in size to ≈5 nm in diameter. The NPs begin to coalesce, and their lattices become sharper (Figure 3D). This is seen also from the diffraction patterns, which show weak and diffuse rings at low temperature, and sharp and more numerous rings at increased temperatures (Figure 4C and 4D, respectively).

Irradiation of solutions at pH = 4.0 form NPs that are significantly different from lower pH samples. The NPs (≈ 6.0 nm in length) are long, rod-shaped NPs. As the particles sinter (heating to 600 °C), holes form between the rod-like particles in the aggregates (Figures 3F and 5). The holes formed are likely indicative of condensation reactions in which −OH groups bound to adjacent uranium ions react to form water and a bridging oxo ligand; the presence of hydroxide ions is anticipated by the Pourbaix diagram in the region of pH = 4. Upon heating under vacuum the water evaporates, the rods lose mass, and the final crystalline product has the morphology of a porous aggregate. As with the NPs formed at the lower pH values of 1.5 and 3.0, the diffraction pattern for the as-synthesized NPs is weaker and more diffuse at RT (Figure 4E). After heating, the diffraction patterns of the rod-like NPs grow stronger and exhibit more diffraction rings (Figure 4F).

The lattice spacings in the NPs are measured from the sample diffraction patterns shown in Figure 4. The reported

dx.doi.org/10.1021/cm2020669 | Chem. Mater. 2011, 23, 5185–5190

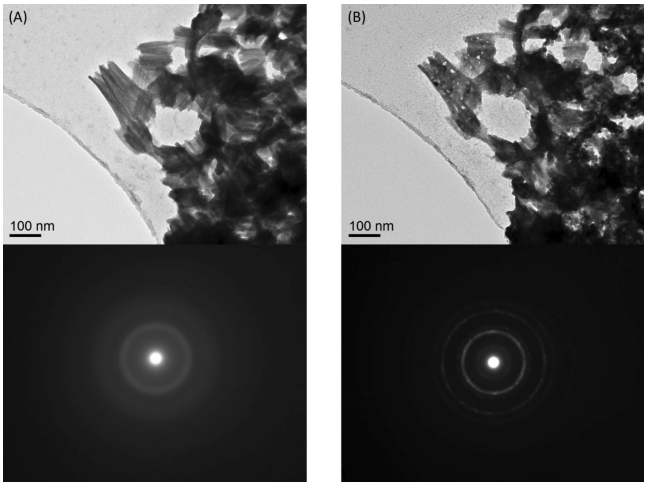

Figure 5. TEM image of in situ heating experiment for UO_2 at pH = 4.0, (A) before heating with corresponding diffraction pattern, and (B) after heating to 600 °C with holes present between the rod-like particles in the aggregates, with corresponding diffraction pattern.

literature lattice spacings for UO_2,[22,23] and the lattice spacings for both RT and sintered NPs from solutions at pH = 1.5, 3.0, and 4.0, respectively, are shown in Table 1. The measured lattice spacings for all samples, before and after heating, correspond with the spacings reported in the literature for UO_2. The small deviations at pH 4 are likely due to the presence of U(VI) hydroxide impurities, as described above. These decrease upon heating, as would be expected from hydroxide species that react to form denser oxides.

The NPs phase and oxidation state were confirmed by close examination of the diffraction data to be that of UO_2. As can be seen from Supporting Information, Table S1, the calculated diffraction data for UO_{2+x}, U_4O_9 and U_3O_8 phases contain large *d*-spacings. These *d*-spacings cannot be fit to our experimental data. Therefore, through the combination of the diffraction data with the UV−vis data and pH conditions of the reactions, the product phases are assigned as UO_2.

CONCLUSION

With an interest toward the recycling and reuse of dissolved uranium oxide from spent nuclear fuels, we are studying the controlled RT formation of UO_2 NPs by radiolysis. A combination of UV−vis, RT TEM, and in situ high temperature stage TEM allowed for detailed analysis of the reaction yield, product composition, and sintering behavior of the NPs formed. The ability to have a high yield of pure UO_2 NPs allows for the subsequent low-temperature sintering of the NPs to usable bulk UO_2 mixed oxide, with reduced defects and better composition control.

Our studies confirm that RT radiolysis of uranyl nitrate solutions will form pure uranium oxide (UO_2) NPs. The reaction is pH dependent; with the optimal reaction at pH = 4.0. At this pH, a relatively stable suspension of sub-10 nm particles is formed in solution, resulting in the reaction proceeding to completion. This is confirmed by UV−vis. Interestingly, there is evidence of a small quantity of hydroxyl groups present on the as-synthesized NPs.

By comparison, a number of reaction conditions will adversely affect the production and yield of the UO_2 NPs. For example, reactions at lower pH (1.2 and 3.0) will produce UO_2 NPs. However, the yield is decreased (e.g., yields of 70% and 79%, respectively) as evidenced by the remaining presence of ionic precursor in solution post-irradiation. Furthermore, our experiments indicate that the presence of chloride (pH = 1.5) anion versus nitrate (pH = 1.2) in the reaction solution will interfere with the reduction of uranyl ion and results in minimizing the conversion yield of UO_2^{2+} to UO_2 via radiolysis (yields = 17% vs 79%, respectively).

Importantly, all UO_2 NPs formed by radiolysis are able to be sintered at extremely low temperatures of 500 °C−600 °C, which is between 700−1000 °C lower than reported bulk sintering temperatures for this material. These initial results suggest a promising path toward a low-temperature method to reuse dissolved actinides from spent nuclear fuels. Our ongoing studies include the synthesis via radiolysis, characterization, and low temperature sintering of uranium metal and alloys NPs.

ASSOCIATED CONTENT

Supporting Information

Further details are given in Figure S1 and Table S1. This material is available free of charge via the Internet at http://pubs.acs.org.

Table 1. Lattice Spacings from Reported[22,23] Values of UO_2, and Calculated Values for UO_2 Samples Synthesized at pH 1.5, 3.0, and 4.0[a]

Reported[22] Values UO_2	Reported[23] Values UO_2	pH 1.5 RT	pH 1.5 600 °C	pH 3.0 RT	pH 3.0 500 °C	pH 4.0 RT	pH 4.0 600 °C
41−1422	36−89						
3.15	3.15	3.17	3.12	3.2	3.11	3.25	3.18
2.73	2.7		2.75	2.75	2.72	2.84	2.78
1.93	1.94	1.83	1.93	1.94	1.93	2.08	1.97
			1.65	1.65	1.64		1.69
			1.35				
			1.25				
			1.21				
			1.11				
			1.04				
			0.91				
			0.84				

[a]Experimental values for both before (RT) and after sintering at 600°C for sample at pH = 1.5, at 500 °C for sample at pH = 3.0, and at 600 °C for sample at pH = 4.0.

dx.doi.org/10.1021/cm2020669 | *Chem. Mater.* 2011, 23, 5185−5190

AUTHOR INFORMATION

Corresponding Author
*E-mail: tmnenof@sandia.gov.

ACKNOWLEDGMENTS

We acknowledge financial support from Sandia's Laboratory Directed Research and Development (LDRD) program.

Sandia National Laboratories is a multiprogram laboratory managed and operated by Sandia Corporation, a wholly owned subsidiary of Lockheed Martin Corporation, for the U.S. Department of Energy's National Nuclear Security Administration under contract DE-AC04-94AL85000.

REFERENCES

(1) Belloni, J.; Mostafavi, M.; Remita, H.; Marignier, J. L.; Delcourt, M. O. *New J. Chem.* **1998**, *22*, 1239.
(2) Ferrando, R.; Jellinek, J.; Johnston, R. L. *Chem. Rev.* **2008**, *108*, 845.
(3) Zhang, Z.; Nenoff, T.; Leung, K.; Ferreira, S.; Huang, J.; Berry, D.; Provencio, P.; Stumpf, R. *J. Phys. Chem. C* **2010**, *114*, 14309.
(4) Zhang, Z. Y.; Nenoff, T. M.; Huang, J. Y.; Berry, D. T.; Provencio, P. P. *J. Phys. Chem. C* **2009**, *113*, 1155.
(5) Leung, K.; Jiao, D.; Rempe, S. B.; Nenoff, T. M. *J. Chem. Theory Comput.* **2011**, *7*, 485.
(6) Burns, P. C. *Cr. R. Chim.*, **2010**, *13*, 737; and references therein.
(7) Suzuki, T.; Abdelouas, A.; Grambow, B.; Mennecart, T.; Blondiaux, G. *Radiochim. Acta* **2006**, *94*, 567.
(8) Atinault, E.; De Waele, V.; Fattahi, M.; LaVerne, J.; Pimblott, S.; Mostafavi, M. *J. Phys. Chem. A* **2009**, *113*, 949.
(9) Atinault, E.; De Waele, V.; Belloni, J.; Le Naour, C.; Fattahi, M.; Mostafavi, M. *J. Phys. Chem. A* **2010**, *114*, 2080.
(10) Roth, O.; Hasselberg, H.; Jonsson, M. *J. Nucl. Mater.* **2009**, *383*, 231.
(11) Bard, A. J.; Parsons, R.; Jordan, J. *Standard Potentials in Aqueous Solutions*, IUPAC; Marcel Dekker: New York, 1985.
(12) Bowen, P.; Carry, C. *Powder Technol.* **2002**, *128*, 248.
(13) Chaim, R.; Levin, M.; Shlayer, A.; Estournes, C. *Adv. Appl. Ceram.* **2008**, *107*, 159.
(14) Trunec, M.; Maca, K. *J. Am. Ceram. Soc.* **2007**, *90*, 2735.
(15) Muroi, M.; Trotter, G.; McCormick, P. G.; Kawahara, M.; Tokita, M. *J. Mater. Sci.* **2008**, *43*, 6376.
(16) Joung, C. Y.; Lee, S. C.; Kim, S. H.; Kim, H. S.; Sohn, D. S. *J. Nucl. Mater.* **2008**, *375*, 209.
(17) Bel, A.; Delmas, R.; Francois, B. *J. Nucl. Mater.* **1959**, *1*, 259.
(18) Robinson, D. B.; Langham, M. E.; Fares, S. J.; Ong, M. D.; Jacobs, B. W.; Clift, W. M.; Murton, J. K.; Hjelm, R. P.; Kent, M. S. *Int. J. Hydrogen Energy* **2010**, *35*, 5423.
(19) Meinrath, G. *J. Radioanal. Nucl. Chem.* **1997**, *224*, 119.
(20) Pourbaix, M. *Atlas of Electrochemical Equilibria in Aqueous Solutions*; National Association of Corrosion Engineers, 1974.
(21) Olsson, M.; Jakobsson, A. M.; Albinsson, Y. *J. Colloid Interface Sci.* **2002**, *256*, 256.
(22) Powder Diffraction File, Card No. 41-1422. International Centre for Diffraction Data: Newtown Square, PA.
(23) Powder Diffraction File, Card No. 36-89. International Centre for Diffraction Data: Newtown Square, PA.